Data report: hysteresis properties of igneous rocks from Holes U1439C, U1440B, and U1442A

Claire Carvallo

Reagan, M.K., Pearce, J.A., Petronotis, K.E., and the Expedition 352 Scientists
Proceedings of the International Ocean Discovery Program Volume 352
publications.iodp.org

doi:10.14379/iodp.proc.352.201.2017

Data report: hysteresis properties of igneous rocks from Holes U1439C, U1440B, and U1442A[1]

Claire Carvallo[2]

Keywords: International Ocean Discovery Program, IODP, *JOIDES Resolution*, Expedition 352, Izu-Bonin-Mariana Fore Arc, Site U1439, Site U1440, Site U1442, hysteresis parameters, rock magnetism

Contents

Abstract

Hysteresis loops and direct current backfield curves were measured on 146 samples from Hole U1439C, 54 samples from Hole U1440B, and 56 samples from Hole U1442A, which were cored during International Ocean Discovery Program Expedition 352. Saturation magnetization values correlate fairly well with the downhole lithology. For samples from Holes U1439C and U1442A, hysteresis parameters plot in different regions of the Day plot depending on whether their composition is boninitic or andesitic. Similarly in Hole U1440B, samples from the various petrologic units plot have different hysteresis parameters. The results show that the magnetic mineralogy varies strongly within each hole.

Introduction

International Ocean Discovery Program (IODP) Expedition 352 took place August–September 2014 and was aimed at studying oceanic crustal accretion immediately following subduction initiation by drilling into the Izu-Bonin-Mariana (IBM) fore arc. The IBM system is sufficiently old that it carries a full record of the evolution of crustal accretion from the start of subduction to the start of normal arc volcanism and sufficiently young that the key features have not been excessively disturbed by subsequent erosion or deformation. Expedition 352 successfully cored 1.22 km of igneous basement and 0.46 km of overlying sediment, providing diverse, stratigraphically controlled suites of fore-arc basalt (FAB) and boninites related to seafloor spreading and earliest arc development. FAB and related rocks were recovered at the two deeper water sites (U1440 and U1441), and boninites and related rocks were recovered at the two sites drilled upslope to the west (Sites U1439 and U1442). Holes U1439C and U1442A yielded entirely boninite differentiation–series lavas that generally become more primitive and have lower TiO_2 concentrations uphole.

Thermal and alternating field (AF) demagnetizations were carried out by the shipboard paleomagnetists on discrete samples in order to give an estimate of the inclination of the recorded geomagnetic field. These shipboard results were reported in the Paleomagnetism sections of each site chapter. In order to carry out more detailed paleomagnetic studies, more samples were collected as paleomagnetic cubes or minicores in Holes U1439C, U1440B, and U1440A for thermal and AF demagnetizations to be carried out on shore. To better understand the magnetic mineralogy of the sampled flows, a slice of sample from the bottom of each cube or minicore was collected for hysteresis measurements. Some results will be presented in Carvallo et al. (in prep.), but that study will focus on a few samples that were selected for the paleointensity study. Hysteresis measurements were subsequently made on the larger suite of samples and are presented here.

Methods and materials

Hysteresis measurements were carried out at Institut de Physique du Globe de Paris–Institut de Minéralogie, de Physique des Matériaux et de Cosmochimie (IPGP-IMPMC) Mineral Magnetism Analytical Facility with a magnetometer (μ-VSM) from Princeton Measurements Corporation. A millimeter-size chip (between 100 and 800 mg) was fixed on the probe with grease. A maximum field of 1 T was applied, and the averaging time was 100 ms. When the magnetization was weak (as it is often the case for boninite) and therefore the hysteresis loops were noisy, between 5 and 20 loops were then measured and averaged together. Hysteresis loops were corrected for the diamagnetic and paramagnetic contribution, and the remanent magnetization (M_r), saturation magnetization (M_s), and coercivity field (H_c) parameters were calculated from the corrected loops. Backfield direct current curves were also measured for each sample in order to obtain the remanent coercivity field (H_{cr}).

[1] Carvallo, C., 2017. Data report: hysteresis properties of igneous rocks from Holes U1439C, U1440B, and U1442A. *In* Reagan, M.K., Pearce, J.A., Petronotis, K.E., and the Expedition 352 Scientists, *Izu-Bonin-Mariana Fore Arc*. Proceedings of the International Ocean Discovery Program, 352: College Station, TX (International Ocean Discovery Program). http://dx.doi.org/10.14379/iodp.proc.352.201.2017

[2] Institut de Minéralogie, de Physique des Matériaux et de Cosmochimie, UPMC Univ Paris 06, UMR CNRS 7590, MNHN, IRD UMR 206, 4 Place Jussieu, F-75005 Paris, France.
carvallo@impmc.upmc.fr

MS 352-201: Received 16 June 2016 · Accepted 11 November 2016 · Published 31 January 2017

Results

Hole U1439C

A total of 146 hysteresis parameters were measured for samples from Hole U1439C. Results are summarized in Table **T1**. All parameters span a very large range. For instance, M_s values span 3 orders of magnitude, from 10^{-3} to 1 Am^2/kg, and H_c ranges from 2 to 35 mT. When plotted downhole, M_r and M_s values show some correlation with petrologic units (Figure **F1A, F1B**). These values are the highest in Units 5, 7, 8b, and 10 and in some parts in Units 6 and 8c. This also corresponds to where onboard bulk magnetic susceptibility was found to be highest. Units 7, 8b, and 10 correspond to andesite, but the high values found in the boninite units could be caused by secondary alteration (see **Petrology** in the Site U1439 chapter [Reagan et al., 2015a]). H_c and H_{cr} values do not show such a correlation with the petrologic units (Figure **F1D, F1F**). Because of this correlation between M_s and lithology, M_s as a function of the MgO, TiO_2, and Al_2O_3 concentrations from the portable X-ray fluores-

Table T1. Hysteresis parameters for samples from Hole U1439C. M_r = remanent magnetization, M_s = saturation magnetization, H_c = coercive field, H_{cr} = remanent coercivity field. (Continued on next page.) **Download table in .csv format.**

Core, section, interval (cm)	M_r (Am^2/kg)	M_s (Am^2/kg)	M_r/M_s	H_c (mT)	H_{cr} (mT)	H_{cr}/H_c
352-U1439C-						
2R-3, 34–36	1.08E–03	4.90E–03	0.220	17.97	28.70	1.60
3R-1, 41–43	4.46E–04	2.70E–03	0.165	17.49	26.09	1.49
4R-1, 45–47	5.63E–03	2.03E–02	0.277	29.86	76.68	2.57
5R-2, 42–44	4.06E–04	2.79E–03	0.146	21.12	55.25	2.62
7R-1, 36–38	1.18E–02	5.37E–02	0.219	20.75	47.05	2.27
7R-1, 58–60	7.28E–04	4.64E–03	0.157	16.35	56.21	3.44
8R-1, 143–145	3.04E–04	1.85E–03	0.165	17.63	54.18	3.07
8R-2, 85–87	5.48E–02	7.22E–01	0.076	4.25	15.74	3.70
10R-1, 10–12	5.49E–02	4.60E–01	0.119	6.47	17.43	2.69
10R-2, 9–11	6.34E–02	6.52E–01	0.097	5.72	17.15	3.00
10R-2, 53–55	2.52E–02	9.34E–02	0.269	14.86	27.71	1.86
11R-1, 8–10	2.40E–02	2.21E–01	0.109	5.93	15.66	2.64
11R-1, 62–64	3.77E–02	1.49E–01	0.253	13.29	23.84	1.79
11R-2, 88–90	2.70E–02	2.47E–01	0.109	5.86	17.01	2.90
11R-2, 126–128	5.31E–02	5.64E–01	0.094	5.14	15.77	3.07
12R-1, 15–17	6.24E–02	6.42E–01	0.097	5.34	15.32	2.87
12R-1, 56–58	4.65E–02	5.14E–01	0.090	5.54	17.47	3.16
12R-1, 84–86	3.09E–02	1.17E–01	0.264	13.88	24.87	1.79
12R-1, 102–104	4.16E–02	4.23E–01	0.098	5.33	15.53	2.91
13R-1, 10–12	2.36E–02	1.31E–01	0.180	9.40	19.72	2.10
13R-1, 113–115	3.67E–02	2.58E–01	0.142	7.24	17.46	2.41
14R-2, 35–37	1.41E–03	9.46E–03	0.149	8.08	21.78	2.70
15R-1, 84–86	3.32E–03	1.17E–02	0.285	28.59	80.05	2.80
15R-1, 113–115	2.63E–03	1.15E–02	0.229	13.08	33.03	2.53
15R-1, 126–128	1.32E–02	5.77E–02	0.229	15.99	33.33	2.08
15R-2, 9–11	1.15E–03	5.73E–03	0.201	20.66	46.72	2.26
15R-2, 36–38	2.59E–03	1.00E–02	0.258	25.02	47.48	1.90
15R-2, 50–52	1.10E–03	5.78E–03	0.190	20.78	58.15	2.80
16R-1, 53–55	2.85E–03	1.17E–02	0.244	24.30	51.44	2.12
16R-1, 73–75	6.05E–04	3.93E–03	0.154	13.22	34.68	2.62
16R-1, 87–89	8.24E–04	4.87E–03	0.169	14.31	31.22	2.18
16R-1, 130–132	5.47E–04	3.49E–03	0.156	16.03	32.96	2.06
16R-2, 45–47	4.75E–04	3.30E–03	0.144	18.98	43.35	2.28
16R-2, 87–89	1.23E–03	5.65E–03	0.218	28.96	62.12	2.15
16R-3, 106–108	2.71E–04	2.01E–03	0.135	14.29	46.97	3.29
18R-1, 92–94	1.53E–03	6.81E–03	0.225	17.30	31.00	1.79
18R-1, 126–128	2.33E–03	1.13E–02	0.206	8.46	25.44	3.01
18R-2, 90–92	5.64E–03	2.08E–02	0.271	23.57	56.70	2.41
18R-2, 122–124	2.99E–03	1.32E–02	0.227	14.87	36.47	2.45
19R-1, 24–26	3.11E–02	1.56E–01	0.200	11.03	23.30	2.11
19R-1, 104–106	8.15E–04	6.61E–03	0.123	8.25	34.62	4.20
19R-2, 58–60	2.28E–02	8.30E–02	0.275	21.90	43.45	1.98
19R-2, 130–132	4.58E–02	3.39E–01	0.135	7.61	19.72	2.59
19R-3, 24–26	3.49E–02	2.33E–01	0.150	8.05	20.42	2.54
19R-3, 80–82	8.50E–03	2.69E–02	0.316	29.46	51.82	1.76
19R-3, 94–96	3.03E–02	1.31E–01	0.231	13.02	26.39	2.03
19R-4, 22–24	2.84E–02	3.21E–01	0.088	4.30	13.67	3.18
19R-4, 63–65	7.93E–03	2.46E–02	0.323	29.71	77.89	2.62
19R-4, 115–117	5.34E–03	2.01E–02	0.266	14.17	32.74	2.31
20R-1, 43–45	6.36E–03	2.12E–02	0.300	26.99	53.45	1.98
20R-1, 82–84	4.33E–06	1.50E–02	0.000	33.33	73.50	2.21
20R-2, 4–6	8.02E–04	4.03E–03	0.199	19.97	39.46	1.98
22R-1, 48–50	6.41E–03	2.22E–02	0.289	21.44	52.88	2.47
22R-1, 103–105	1.06E–02	3.36E–02	0.315	21.05	40.89	1.94
23R-1, 27–29	4.20E–03	1.65E–02	0.255	20.17	41.61	2.06
23R-1, 82–84	4.86E–03	1.59E–02	0.305	18.48	38.76	2.10
23R-2, 31–33	3.96E–02	2.90E–01	0.136	8.03	20.36	2.53
24R-1, 35–37	5.03E–02	4.55E–01	0.111	6.03	17.18	2.85
25R-1, 108–110	1.02E–01	3.54E–01	0.287	13.51	20.91	1.55
25R-2, 16–18	3.17E–03	1.37E–02	0.232	20.72	52.31	2.52
26R-1, 55–57	2.50E–03	1.08E–02	0.230	21.62	61.00	2.82
26R-1, 68–70	7.21E–04	3.86E–03	0.187	16.99	34.47	2.03
26R-1, 72–74	3.96E–03	1.66E–02	0.238	14.81	39.12	2.64
26–2, 24–26	1.05E–03	6.20E–03	0.169	17.51	42.81	2.44
26R-2, 34–36	5.99E–03	1.69E–02	0.355	21.32	41.06	1.93
26R-2, 45–47	4.16E–02	2.54E–01	0.164	8.46	19.21	2.27
26R-3, 12–14	2.16E–02	1.17E–01	0.184	8.52	19.80	2.33
27R-2, 47–49	8.80E–03	3.46E–02	0.254	15.58	30.06	1.93
27R-2, 131–133	1.42E–04	1.27E–03	0.111	9.41	37.64	4.00
27R-3, 2–4	2.09E–03	8.52E–03	0.245	19.20	35.70	1.86
27R-3, 21–23	3.84E–04	3.02E–03	0.127	10.89	63.47	5.83
28R-1, 97–99	1.38E–05	1.19E–03	0.012	0.01	0.02	3.09
28R-2, 4–6	1.62E–08	4.73E–07	0.034	8.01	21.90	2.74
28R-2, 113–115	1.68E–05	1.09E–03	0.016	6.77	22.57	3.33
28R-3, 16–18	1.94E–06	8.67E–03	0.000	25.29	56.38	2.23
28R-3, 54–56	2.30E–03	8.00E–03	0.288	21.84	50.00	2.29
29R-1, 48–50	1.87E–03	6.97E–03	0.269	29.02	64.98	2.24
29R-1, 92–94	3.85E–03	1.32E–02	0.291	29.85	63.14	2.12
29R-2, 18–20	5.47E–02	5.94E–01	0.092	5.70	16.73	2.94
29R-2, 39–41	1.03E–01	9.14E–01	0.112	6.86	21.12	3.08
29R-2, 67–69	3.85E–02	5.67E–01	0.068	4.72	19.98	4.23
29R-2, 84–86	5.77E–02	6.73E–01	0.086	5.41	17.71	3.27
29R-2, 93–95	6.16E–02	7.18E–01	0.086	5.50	17.63	3.21
29R-3, 8–10	6.48E–02	7.73E–01	0.084	5.24	17.45	3.33
29R-3, 25–27	6.24E–02	5.97E–01	0.104	6.28	17.22	2.74
29R-3, 55–57	4.63E–02	5.51E–01	0.084	5.22	15.24	2.92
29R-3, 110–112	1.05E–01	8.46E–01	0.124	6.79	17.98	2.65
29R-4, 2–4	6.02E–02	6.99E–01	0.086	4.82	14.75	3.06
29R-4, 49–51	1.33E–02	4.53E–02	0.294	23.15	45.79	1.98
29R-5, 4–6	2.21E–05	1.00E–03	0.022	2.18	17.45	8.00
29R-5, 103–105	1.44E–03	6.29E–03	0.229	24.56	53.47	2.18
30R-1, 26–28	3.29E–03	1.24E–02	0.266	29.44	65.33	2.22
30R-1, 131–133	2.81E–03	9.85E–03	0.285	17.90	39.65	2.22
30R-2, 8–10	3.13E–03	1.05E–02	0.298	31.77	69.25	2.18
30R-2, 73–75	1.66E–03	7.62E–03	0.218	16.26	34.99	2.15
30R-3, 10–12	2.53E–03	9.20E–03	0.275	14.01	28.35	2.02
31R-1, 6–8	1.11E–03	4.38E–03	0.254	21.87	58.68	2.68
31R-1, 88–90	3.68E–03	1.44E–02	0.255	18.85	36.68	1.95
31R-2, 47–49	1.14E–03	4.51E–03	0.254	21.09	53.46	2.53
31R-2, 86–88	5.33E–03	2.07E–02	0.258	20.21	38.81	1.92
31R-2, 104–106	1.53E–03	6.01E–03	0.254	22.92	40.57	1.77
31R-2, 118–120	1.61E–03	5.80E–03	0.277	21.19	50.85	2.40
31R-3, 13–15	1.63E–03	7.28E–03	0.224	16.27	40.64	2.50
31R-3, 33–35	1.05E–03	4.38E–03	0.239	25.37	58.13	2.29
31R-3, 39–41	1.04E–03	4.68E–03	0.223	27.17	70.87	2.61
31R-3, 57–59	4.17E–03	1.26E–02	0.330	33.61	79.77	2.37
31R-3, 74–76	2.69E–03	9.83E–03	0.274	19.67	37.68	1.92
31R-3, 137–139	2.58E–03	8.43E–03	0.306	34.39	75.67	2.20
31R-4, 20–22	9.80E–05	1.87E–03	0.052	15.40	71.46	4.64

Table T1 (continued).

Core, section, interval (cm)	M_r (Am²/kg)	M_s (Am²/kg)	M_r/M_s	H_c (mT)	H_{cr} (mT)	H_{cr}/H_c
31R-4, 106–108	3.45E–02	3.60E–01	0.096	4.55	15.12	3.32
31R-5, 22–24	3.21E–02	3.17E–01	0.101	4.89	15.04	3.08
31R-5, 70–72	9.94E–04	4.42E–03	0.225	16.84	38.99	2.32
32R-1, 33–35	3.45E–03	1.36E–02	0.253	20.24	41.19	2.04
32R-1, 85–87	1.22E–03	5.18E–03	0.236	24.10	63.42	2.63
32R-2, 12–14	6.65E–03	2.14E–02	0.310	26.20	48.76	1.86
32R-2, 48–50	4.21E–02	2.08E–01	0.202	10.41	21.03	2.02
32R-3, 84–86	8.18E–05	1.40E–03	0.058	9.00	26.29	2.92
32R-3, 110–112	1.92E–03	7.46E–03	0.257	23.13	45.67	1.97
32R-4, 40–42	6.73E–04	3.84E–03	0.176	14.29	45.09	3.16
32R-4, 64–66	1.48E–03	5.95E–03	0.249	14.72	35.34	2.40
32R-4, 135–137	7.42E–04	3.16E–03	0.235	32.21	87.46	2.72
32R-4, 140–142	2.02E–03	7.27E–03	0.277	34.11	84.48	2.48
32R-5, 3–5	4.25E–04	2.22E–03	0.192	25.43	52.89	2.08
33R-1, 64–66	2.77E–04	1.88E–03	0.148	10.97	44.16	4.03
33R-1, 80–82	3.83E–04	2.14E–03	0.179	16.48	24.45	1.48
35R-1, 82–84	2.27E–03	9.49E–03	0.239	15.21	36.32	2.39
35R-1, 114–116	4.50E–03	1.62E–02	0.279	17.71	34.63	1.96
35R-2, 72–74	1.97E–02	8.51E–02	0.231	17.11	37.46	2.19
35R-2, 121–123	1.29E–03	5.52E–03	0.233	19.22	49.78	2.59
35R-3, 2–4	1.44E–03	5.34E–03	0.270	23.34	43.49	1.86
35R-3, 115–117	3.75E–04	2.34E–03	0.161	12.41	28.57	2.30
39R-1, 92–94	5.71E–02	5.32E–01	0.107	6.12	15.72	2.57
39R-2, 37–39	4.99E–02	2.67E–01	0.187	11.71	25.27	2.16
39R-2, 62–64	1.73E–02	7.50E–02	0.230	13.00	31.40	2.42
39R-2, 123–125	9.06E–02	7.62E–01	0.119	7.06	17.12	2.43
39R-2, 135–137	6.51E–02	5.98E–01	0.109	6.66	17.72	2.66
39R-3, 28–30	6.75E–02	6.99E–01	0.097	5.63	15.61	2.77
39R-3, 53–55	3.90E–02	4.55E–01	0.086	5.10	15.65	3.07
39R-3, 70–72	5.05E–02	5.38E–01	0.094	5.59	15.03	2.69
40R-1, 14–16	4.24E–02	4.15E–01	0.102	6.16	16.99	2.76
40R-1, 29–31	5.69E–02	7.17E–01	0.079	4.31	13.03	3.02
40R-1, 83–85	2.20E–02	9.27E–02	0.238	14.84	27.87	1.88
40R-1, 102–104	7.66E–02	4.15E–01	0.185	10.37	19.68	1.90
40R-2, 3–5	8.20E–02	6.43E–01	0.128	7.63	17.85	2.34
40R-2, 112–114	7.59E–02	7.18E–01	0.106	7.63	17.85	2.34
41R-1, 86–87	4.64E–02	6.27E–01	0.074	4.09	10.03	2.45

Figure F1. A–F. Hysteresis parameters vs. depth, Hole U1439C. Petrologic units are described in the **Site U1439** chapter (Reagan et al., 2015a).

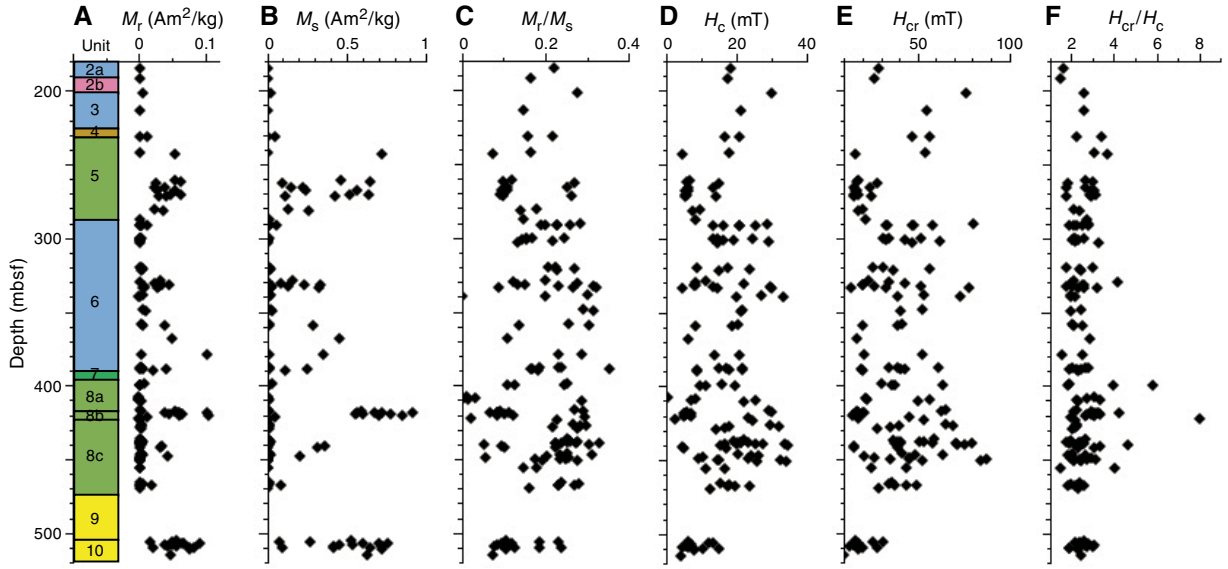

cence measurements carried out on board was also plotted for samples as close as possible (≤60 cm) to samples used for hysteresis measurement. M_s seems to be higher when Al_2O_3 and TiO_2 concentrations are higher and MgO concentrations are lower (Figure **F2**).

A few samples have a very low M_r/M_s ratio (<0.050), but most of them are between 0.050 and 0.350. Some H_{cr}/H_c ratios are very high, but they correspond to very weak samples and therefore might not be reliable. The hysteresis parameters were plotted on a Day plot (Day et al., 1977) with Dunlop (2002) mixing lines and were separated into two categories: weak samples (M_s < 0.1 Am²/kg) and strong samples (M_s > 0.1 Am²/kg). These two categories plot in different regions on the Day plot. The strong samples follow the single-domain–multidomain (SD–MD) mixing line, but the weak samples are between the SD–MD and single-domain–superparamagnetic (SD–SP) mixing line, suggesting that the two groups have different magnetic mineralogies (Figure **F3**).

Hole U1440B

Fifty-four hysteresis parameters were measured on samples from Hole U1440B. Results are summarized in Table **T2**. M_s values are strong, between 0.3 and 2 Am²/kg (except for one very weak sample that might have been misnamed). The hysteresis parameters show fairly good correlation with the petrologic units defined in the **Site U1440** chapter (Reagan et al., (2015b) (Figure **F4**). M_r values are higher in the volcanic extrusive zone than in the dikes zone, while it is the opposite for M_s (Figure **F4A, F4B**). H_c and H_{cr} also follow this tendency on average, and H_{cr}/H_c ratios are higher in the dikes zone than in the volcanic extrusive zone (except for the suspicious sample with a very low saturation magnetization) (Figure **F4D, F4F**). When plotted on a Day plot, the samples from the three different units plot in three different regions (Figure **F5**), slightly below the SD–MD mixing line; the volcanic extrusive samples have 60%–100% SD grains, whereas the samples from the dikes unit con-

Figure F2. Saturation magnetization vs. (A) Al_2O_3, (B) TiO_2, and (C) MgO concentrations from portable X-ray fluorescence measurements made on board on parts of Hole U1439C core ≤60 cm away from samples used for hysteresis measurements.

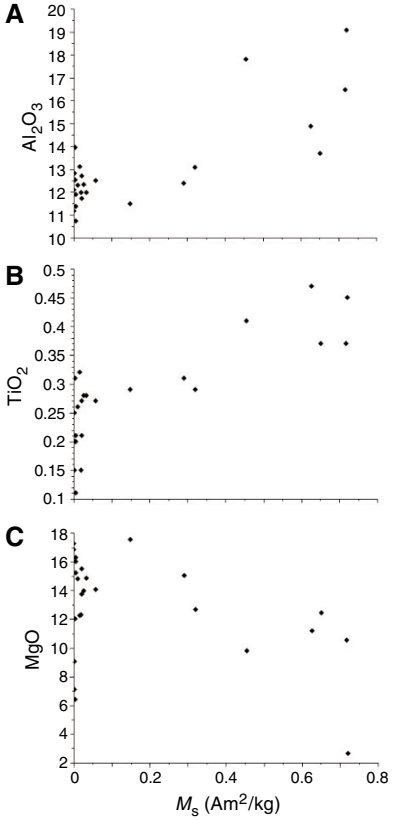

Figure F3. Day plot for samples from Hole U1439C, with the mixing lines of Dunlop (2002). Blue = samples with M_s > 0.1 Am²/kg, green = samples with M_s < 0.1 Am²/kg.

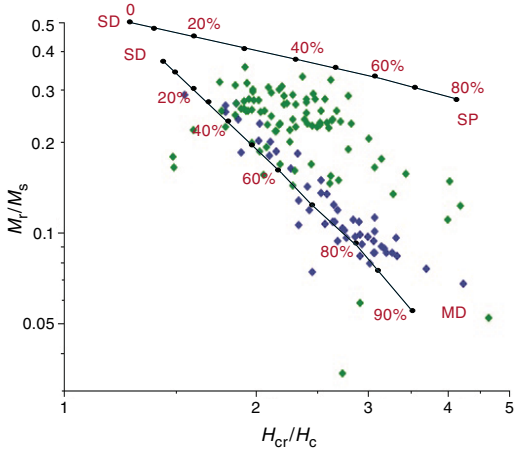

tain between 10% and 60% SD grains. The compositions of samples from the transition zone are intermediate between these two zones.

Hole U1442A

Fifty-six hysteresis loops were measured on samples from Hole U1442A. As expected, the hysteresis parameter values show a large spread, similar to what was observed for Hole U1439C (Table T3).

Table T2. Hysteresis parameters for samples from Hole U1440B. M_r = remanent magnetization, M_s = saturation magnetization, H_c = coercive field, H_{cr} = remanent coercivity field. **Download table in .csv format.**

Core, section, interval (cm)	M_r (Am²/kg)	M_s (Am²/kg)	M_r/M_s	H_c (mT)	H_{cr} (mT)	H_{cr}/H_c
352-U1440B-						
4R-1, 124–126	1.90E–01	5.66E–01	0.336	10.95	15.31	1.40
5R-1, 15–17	1.16E–01	5.17E–01	0.224	8.78	14.44	1.64
6R-1, 34–36	1.71E–01	4.68E–01	0.365	13.19	17.83	1.35
7R-1, 2–4	1.13E–01	3.01E–01	0.376	8.83	13.31	1.51
7R-1, 52–54	1.21E–01	4.02E–01	0.300	8.82	14.49	1.64
8R-1, 28–30	1.49E–01	4.53E–01	0.330	11.51	16.53	1.44
8R-1, 39–41	1.49E–01	4.62E–01	0.323	11.04	15.98	1.45
8R-1, 48–50	1.32E–01	4.62E–01	0.285	8.08	13.59	1.68
8R-1, 58–60	8.28E–05	1.35E–03	0.061	7.70	35.63	4.63
8R-1, 88–90	1.51E–01	5.95E–01	0.254	8.03	13.30	1.66
10R-1, 80–82	1.07E–01	5.18E–01	0.207	6.42	11.59	1.80
11R-1, 38–40	1.31E–01	4.75E–01	0.276	7.78	12.62	1.62
12R-1, 91–93	7.95E–02	3.12E–01	0.255	7.99	13.43	1.68
12R-2, 55–57	7.99E–02	2.95E–01	0.271	7.53	12.47	1.66
12R-2, 134–137	1.88E–01	6.73E–01	0.279	8.73	13.44	1.54
13R-1, 23–25	1.46E–01	4.87E–01	0.300	8.94	13.88	1.55
13R-1, 108–110	1.92E–01	6.29E–01	0.305	9.12	13.50	1.48
14R-1, 26–28	2.03E–01	6.80E–01	0.299	9.31	13.96	1.50
15R-1, 41–43	1.68E–01	6.05E–01	0.277	8.44	13.10	1.55
17R-1, 89–91	1.43E–01	7.76E–01	0.185	6.93	11.73	1.69
18R-1, 21–23	1.47E–01	5.72E–01	0.256	7.47	12.11	1.62
18R-1, 112–114	1.67E–01	6.37E–01	0.262	7.60	12.45	1.64
20R-1, 19–21	1.46E–01	6.02E–01	0.242	7.29	11.28	1.55
21R-1, 81–83	1.78E–01	6.45E–01	0.277	10.58	16.75	1.58
25R-1, 80–82	1.66E–01	6.61E–01	0.251	8.53	12.41	1.46
27R-1, 42–44	1.63E–01	1.67	0.098	5.00	10.84	2.17
27R-1, 52–54	1.71E–01	1.56	0.110	5.08	10.54	2.07
28R-1, 19–21	9.59E–02	1.64	0.058	2.74	47.17	17.23
29R-1, 37–39	1.35E–01	8.32E–01	0.163	5.09	8.79	1.73
32R-1, 8–10	1.21E–01	1.52	0.080	3.79	8.54	2.25
32R-1, 19–21	1.01E–01	1.39	0.073	3.60	8.55	2.37
32R1–, 33–35	1.40E–01	1.06	0.131	5.38	10.23	1.90
32R-1, 39–41	1.74E–04	9.81E–01	0.000	6.90	11.81	1.71
32R-1, 65–67	1.63E–01	1.66	0.098	4.42	9.29	2.10
32R-1, 81–83	1.38E–01	1.46	0.095	4.86	10.32	2.12
32R-1, 94–96	1.12E–01	1.38	0.081	4.07	9.42	2.31
32R-1, 104–106	1.20E–01	1.52	0.079	4.05	9.89	2.44
33R-1, 83–85	1.15E–01	7.81E–01	0.147	5.25	9.87	1.88
35R-1, 18–20	1.02E–01	4.64E–01	0.220	5.47	9.33	1.71
35R-1, 42–44	8.04E–02	4.53E–01	0.177	5.08	9.15	1.80
35R-1, 53–55	8.77E–02	4.48E–01	0.196	5.21	9.14	1.75
35R-1, 58–60	8.44E–02	7.18E–01	0.118	4.21	8.26	1.96
35R-1, 70–71	6.56E–02	8.03E–01	0.082	3.93	9.27	2.36
35R-1, 77–79	6.73E–02	1.06	0.064	3.41	8.52	2.50
35R-1, 82–84	8.03E–02	7.83E–01	0.103	4.31	8.52	1.98
35R-1, 93–94	8.73E–02	1.29	0.068	3.58	9.11	2.54
36R-1, 7–9	8.08E–02	1.74	0.046	2.92	9.08	3.11
36R-1, 17–18	9.37E–02	1.87	0.050	3.02	8.94	2.96
36R-1, 47–49	9.69E–02	1.92	0.051	3.31	10.36	3.13
36R-1, 52–54	1.17E–01	2.36	0.050	3.42	10.98	3.21
36R-1, 60–62	9.08E–02	1.90	0.048	3.04	9.32	3.06
36R-1, 75–77	8.07E–02	1.58	0.051	3.20	9.53	2.98
36R-1, 81–83	7.52E–02	1.41	0.053	3.23	9.16	2.83
36R-1, 95–97	7.21E–02	1.40	0.052	3.23	9.54	2.95

Correlation with the lithology is not as clear as for the other two holes (Figure F6). M_s and M_r values seem to be higher in Unit 2, where dikes could be present among boninite. The very high H_{cr}/H_c ratios come from very weak and noisy samples and therefore have to be regarded with caution. As for Hole U1439C, it is possible to plot Al_2O_3, TiO_2, and MgO concentrations as a function of saturation magnetization (Figure F7). Again, a slight correlation appears: M_s is higher where samples contain more TiO_2 and Al_2O_3 and lower

Figure F4. A–F. Hysteresis parameters vs depth, Hole U1440B. Petrologic units are described in the **Site U1440** chapter (Reagan et al., 2015b).

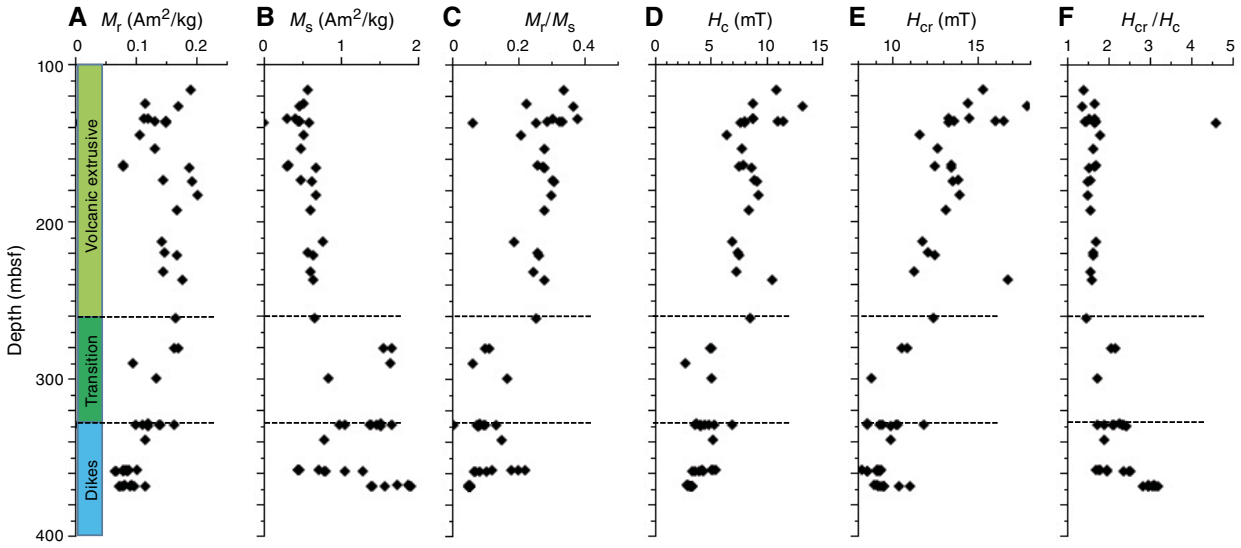

Figure F5. Day plot for samples from Hole U1440B, with the mixing lines of Dunlop (2002). Light green = samples from the volcanic extrusive unit, dark green = samples from the transition unit, blue = samples from the dikes units. Petrologic units are described in the **Site U1440** chapter (Reagan et al., 2015b).

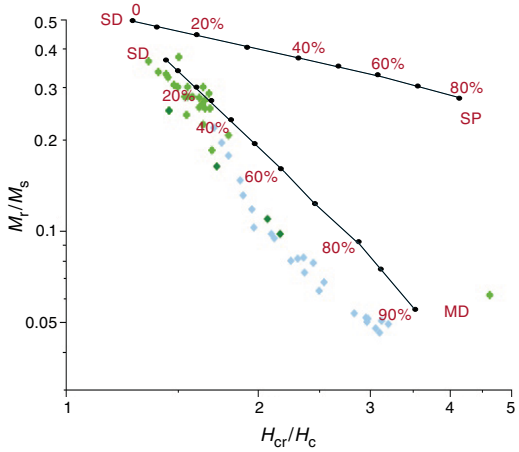

where samples contain more MgO; although this correlation does not appear as clearly as for Hole U1439C. For the Day plot representation (Figure **F8**), samples are again divided into two groups: weak samples (M_s < 0.1 Am^2/kg) and strong samples (M_s > 0.1 Am^2/kg). The difference in hysteresis parameters between the two groups is not as clear as for Hole U1439C. Strong samples have a tendency to plot slightly closer to the SD–MD mixing line than the weak samples, showing again the difference in magnetic mineralogy between the two groups.

Table T3. Hysteresis parameters for samples from Hole U1442A. M_r = remanent magnetization, M_s = saturation magnetization, H_c = coercive field, H_{cr} = remanent coercivity field. **Download table in .csv format.**

Core, section, interval (cm)	M_r (Am^2/kg)	M_s (Am^2/kg)	M_r/M_s	H_c (mT)	H_{cr} (mT)	H_{cr}/H_c
352-U1442A-						
10R-3, 50–52	4.02E–02	3.99E–01	0.101	5.44	18.26	3.36
15R-1, 56–58	5.53E–04	3.16E–03	0.175	14.10	35.73	2.53
15R-1, 83–85	1.97E–03	8.31E–03	0.237	22.87	51.54	2.25
21R-1, 112–114	8.18E–05	1.32E–03	0.062	12.93	37.62	2.91
23R-1, 63–65	4.08E–02	5.82E–01	0.070	5.62	19.95	3.55
23R-1, 75–77	4.29E–02	7.17E–01	0.060	4.57	19.00	4.16
23R-1, 85–87	4.34E–02	6.42E–01	0.068	4.85	20.38	4.20
23R-1, 120–122	3.77E–02	7.01E–01	0.054	3.89	15.81	4.07
23R-1, 131–133	2.45E–02	5.84E–01	0.042	3.10	14.61	4.71
23R-1, 109–111	4.67E–02	6.11E–01	0.076	5.40	23.03	4.26
23R-2, 38–40	2.45E–02	4.28E–01	0.057	5.85	22.64	3.87
24R-1, 75–77	2.45E–02	2.34E–01	0.104	6.93	26.47	3.82
25R-1, 67–69	1.42E–03	7.00E–03	0.202	24.66	55.67	2.26
25R-1, 97–99	3.50E–03	1.65E–02	0.213	21.60	59.30	2.75
28R-1, 14–16	4.93E–03	2.03E–02	0.243	23.22	57.24	2.47
29R-1, 89–91	3.98E–05	1.04E–03	0.038	2.82	31.46	11.17
29R-1, 104–106	6.32E–05	7.55E–04	0.084	17.09	35.32	2.07
30R-1, 38–40	1.32E–04	1.74E–03	0.076	19.93	49.81	2.50
30R-1, 119–121	2.15E–02	8.99E–02	0.239	23.34	52.59	2.25
30R-2, 51–53	5.72E–04	2.62E–03	0.219	35.36	83.74	2.37
30R-3, 4–6	8.45E–04	4.01E–03	0.211	26.51	76.84	2.90
30R-3, 120–122	4.78E–02	3.57E–01	0.134	8.78	22.37	2.55
30R-4, 83–85	6.50E–02	5.47E–01	0.119	7.79	7.86	1.01
31R-1, 47–49	8.44E–02	8.96E–01	0.094	5.30	14.02	2.65
31R-1, 60–62	4.37E–02	6.98E–01	0.063	3.95	13.20	3.34
31R-2, 15–17	7.84E–02	9.46E–01	0.083	4.51	13.71	3.04
33R-1, 10–12	5.87E–02	4.47E–01	0.131	8.02	24.51	3.05
33R-1, 33–35	6.14E–02	4.72E–01	0.130	7.46	10.19	1.37
33R-1, 52–54	5.04E–02	4.56E–01	0.111	5.25	14.95	2.85
33R-1, 79–81	7.61E–02	4.39E–01	0.173	9.74	23.58	2.42
34R-1, 10–12	8.25E–02	7.42E–01	0.111	6.32	17.89	2.83
34R-1, 28–30	5.90E–02	5.93E–01	0.099	5.31	16.83	3.17
36R-1, 17–19	1.22E–01	8.08E–01	0.151	8.74	22.90	2.62
36R-1, 82–84	8.92E–02	6.83E–01	0.131	6.05	17.25	2.85
36R-2, 10–12	5.24E–02	4.43E–01	0.118	4.74	11.72	2.47
36R-2, 71–73	3.60E–02	3.33E–01	0.108	4.71	11.69	2.48
37R-1, 86–88	5.83E–02	1.03	0.057	4.38	16.45	3.75
41R-1, 18–20	5.95E–02	6.75E–01	0.088	3.74	10.78	2.88
41R-1, 42–44	5.99E–02	6.59E–01	0.091	3.66	9.91	2.71
43R-1, 49–51	7.57E–02	1.14	0.066	3.80	12.08	3.18
43R-1, 109–111	7.89E–02	1.27	0.062	4.09	14.59	3.57
43R-1, 121–123	8.37E–02	1.18	0.071	4.37	15.34	3.51
47R-1, 50–52	1.48E–04	1.46E–03	0.101	22.74	73.54	3.23
47R-1, 62–64	8.81E–05	1.37E–03	0.064	11.49	11.00	0.96
48R-1, 8–10	1.70E–04	1.22E–03	0.140	6.52	52.55	8.06
48R-1, 35–37	2.29E–02	6.95E–02	0.330	19.43	35.38	1.82
48R-1, 65–67	8.04E–02	9.18E–01	0.088	5.37	17.21	3.21
48R-1, 96–98	1.11E–04	1.62E–03	0.068	9.91	53.42	5.39
48R-1, 133–135	2.78E–05	6.70E–04	0.042	6.17	60.65	9.83
48R-2, 56–58	5.00E–02	8.48E–01	0.059	3.78	13.59	3.59
49R-1, 103–105	5.51E–02	6.65E–01	0.083	5.56	17.09	3.08
49R-33, 2–4	2.54E–04	1.92E–03	0.132	16.71	54.58	3.27
53R-1, 21–23	3.99E–02	2.27E–01	0.176	14.41	33.85	2.35
54R-1, 28–30	4.31E–02	4.27E–01	0.101	7.68	23.16	3.02
54R-2, 13–15	3.74E–02	7.28E–01	0.051	3.76	14.69	3.91
56R-1, 33–35	1.19E–01	5.06E–01	0.236	18.48	35.10	1.90

Figure F6. A–F. Hysteresis parameters vs depth, Hole U1442A. Petrologic units are described in the **Site U1442** chapter (Reagan et al., 2015c).

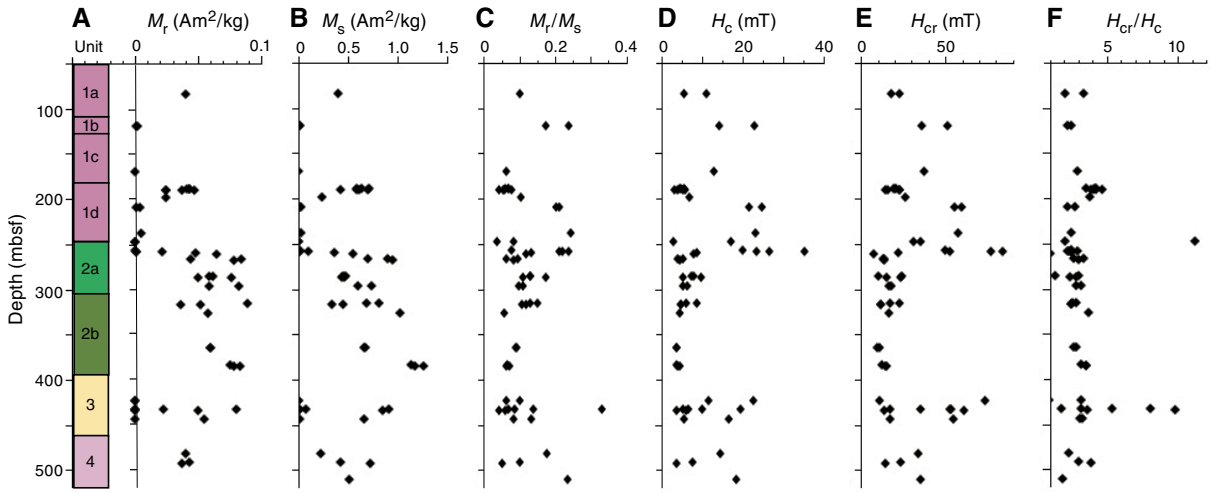

Figure F7. Saturation magnetization vs. (A) Al_2O_3, (B) TiO_2, and (C) MgO concentrations from portable X-ray fluorescence measurements made on board on parts of Hole U1442A core ≤60 cm away from samples used for hysteresis measurements.

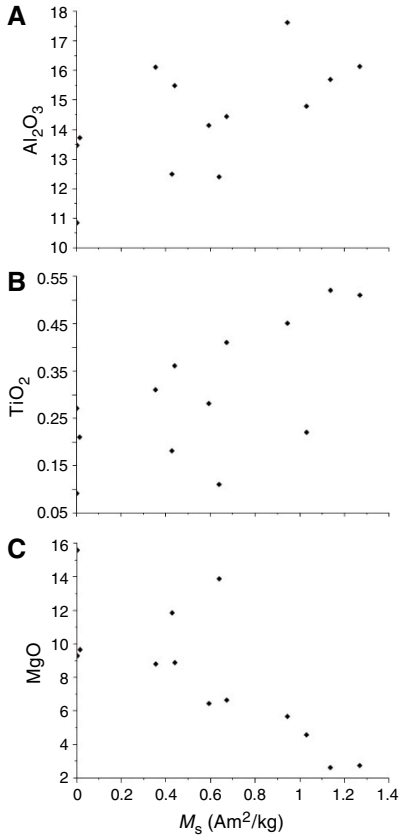

Figure F8. Day plot for samples from Hole U1442A, with the mixing lines of Dunlop (2002). Blue = samples with M_s > 0.1 Am²/kg, green = samples with M_s < 0.1 Am²/kg.

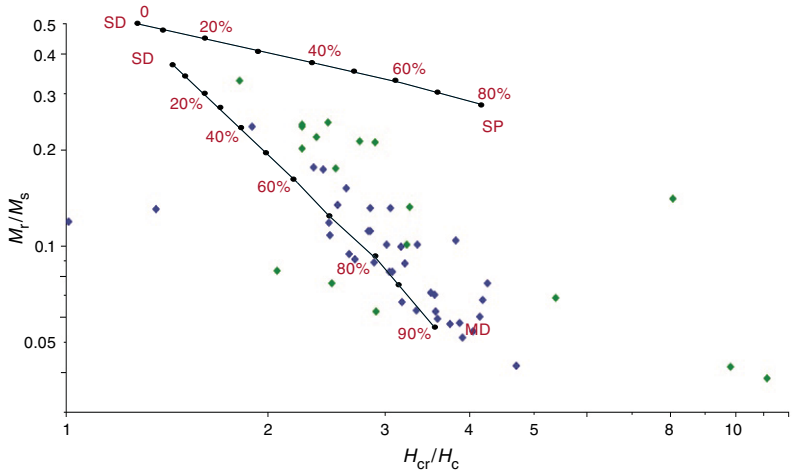

Acknowledgments

This research used samples and data provided by the International Ocean Discovery Program (IODP). IODP France is acknowledged with funding support. I thank F. Lagroix for her help with the measurements, an anonymous reviewer for helpful comments, and IODP for receipt of samples.

References

Day, R., Fuller, M., and Schmidt, V.A., 1977. Hysteresis properties of titanomagnetites: grain-size and compositional dependence. *Physics of the Earth and Planetary Interiors,* 13(4):260–267. **http://dx.doi.org/10.1016/0031-9201(77)90108-X**

Dunlop, D.J., 2002. Theory and application of the Day plot (M_{rs}/M_s versus H_{cr}/H_c), 1. Theoretical curves and tests using titanomagnetite data. *Jour-*

nal of Geophysical Research: Solid Earth, 107(B3):2056. **http://dx.doi.org/10.1029/2001JB000486**

Reagan, M.K., Pearce, J.A., Petronotis, K., Almeev, R., Avery, A.A., Carvallo, C., Chapman, T., Christeson, G.L., Ferré, E.C., Godard, M., Heaton, D.E., Kirchenbaur, M., Kurz, W., Kutterolf, S., Li, H., Li, Y., Michibayashi, K., Morgan, S., Nelson, W.R., Prytulak, J., Python, M., Robertson, A.H.F., Ryan, J.G., Sager, W.W., Sakuyama, T., Shervais, J.W., Shimizu, K., and Whattam, S.A., 2015a. Site U1439. *In* Reagan, M.K., Pearce, J.A., Petronotis, K., and the Expedition 352 Scientists, *Izu-Bonin-Mariana Fore Arc.* Proceedings of the International Ocean Discovery Program, 352: College Station, TX (International Ocean Discovery Program). **http://dx.doi.org/10.14379/iodp.proc.352.103.2015**

Reagan, M.K., Pearce, J.A., Petronotis, K., Almeev, R., Avery, A.A., Carvallo, C., Chapman, T., Christeson, G.L., Ferré, E.C., Godard, M., Heaton, D.E., Kirchenbaur, M., Kurz, W., Kutterolf, S., Li, H., Li, Y., Michibayashi, K., Morgan, S., Nelson, W.R., Prytulak, J., Python, M., Robertson, A.H.F., Ryan, J.G., Sager, W.W., Sakuyama, T., Shervais, J.W., Shimizu, K., and Whattam, S.A., 2015b. Site U1440. *In* Reagan, M.K., Pearce, J.A., Petronotis, K., and the Expedition 352 Scientists, *Izu-Bonin-Mariana Fore Arc.* Proceedings of the International Ocean Discovery Program, 352: College Station, TX (International Ocean Discovery Program). **http://dx.doi.org/10.14379/iodp.proc.352.104.2015**

Reagan, M.K., Pearce, J.A., Petronotis, K., Almeev, R., Avery, A.A., Carvallo, C., Chapman, T., Christeson, G.L., Ferré, E.C., Godard, M., Heaton, D.E., Kirchenbaur, M., Kurz, W., Kutterolf, S., Li, H., Li, Y., Michibayashi, K., Morgan, S., Nelson, W.R., Prytulak, J., Python, M., Robertson, A.H.F., Ryan, J.G., Sager, W.W., Sakuyama, T., Shervais, J.W., Shimizu, K., and Whattam, S.A., 2015c. Site U1442. *In* Reagan, M.K., Pearce, J.A., Petronotis, K., and the Expedition 352 Scientists, *Izu-Bonin-Mariana Fore Arc.* Proceedings of the International Ocean Discovery Program, 352: College Station, TX (International Ocean Discovery Program). **http://dx.doi.org/10.14379/iodp.proc.352.106.2015**